



6-2015

Computer Simulations of Propulsion of Self-Propelled Flexible Nanobody

Ye Luo

Western Michigan University

Follow this and additional works at: https://scholarworks.wmich.edu/masters_theses

 Part of the Chemical Engineering Commons, and the Nanoscience and Nanotechnology Commons

Recommended Citation

Luo, Ye, "Computer Simulations of Propulsion of Self-Propelled Flexible Nanobody" (2015). *Masters Theses*. 603.

https://scholarworks.wmich.edu/masters_theses/603

This Masters Thesis-Open Access is brought to you for free and open access by the Graduate College at ScholarWorks at WMU. It has been accepted for inclusion in Masters Theses by an authorized administrator of ScholarWorks at WMU. For more information, please contact wmu-scholarworks@wmich.edu.



COMPUTER SIMULATIONS OF PROPULSION OF
SELF-PROPELLED FLEXIBLE NANOBODY

by
Ye Luo

A thesis submitted to the Graduate College
in partial fulfillment of the requirements
for the degree of Master of Science in Engineering (Chemical)
Chemical and Paper Engineering
Western Michigan University
June 2015

Thesis committee:

Dewei Qi, Ph.D, Chair
Kalyana C. Pingali, Ph.D
James R. Springstead, Ph.D

COMPUTER SIMULATIONS OF PROPULSION OF SELF-PROPELLED FLEXIBLE NANOBODY

Ye Luo, M. S. E.

Western Michigan University, 2015

Swimming bodies such as flagellum and fishes are found everywhere in liquid environment. The research of simulation of swimmers is one of the most important branches among the field of biophysics. This study focus on the direct computer simulation of self-propelled flexible nanobody in fluid field.

Two new objectives is studied based on the previous research of Tai-hsien Wu and Dewei Qi (2014)[1]. In Wu's article, the front end of micro swimming body is fixed and the migration of swimmers is neglected. For a further study, one of new targets is to release the head in 3-D simulation fluid area. Then the swimming body will gain thrust through the flapping of the filament. Besides, the flapping mode shape with high Reynolds number is worth to study since seldom articles can be utilized. Furthermore, another new objective is that two-body system will be introduced. In this study, we focus on the tandem configuration and the front swimmer influence on the rear one through interaction of flow distribution. Simulation results of single fiber and two-body system is in keeping with previous studies very well.

For the theoretical support in this research, Lattice Boltzmann Method, General Lattice Spring Model and Immersed-boundary Method are introduced to respectively simulate structure of fluid, solid and interaction between fluid and solid.

Copyright by
Ye Luo
2015

ACKNOWLEDGEMENTS

Dr. Qi, Dewei is the supervisor of my graduate thesis. I have followed him and began my research career since fall, 2012, the first year when I arrived Kalamazoo. I admire his enthusiasm of academic and the spirit of concentration. He helps me a lot and encourages me a lot. Without him, I could not image what my research career would be like. I do appreciate for his giving and support.

Dr. Pinagli, Kalyana and Dr. Springstead, James are two other committee members of my thesis. They are also instructors of my graduate courses. Mr. Pingali also teaches CHEG 6600, Methods of research and engineering communication. I learn a lot about how to write a successful research paper. I would like to thank both of them for their assistance.

I especially want to thank Tai-hsien Wu (Bruce), who did lots of previous work for this research including mathematic modeling and the program build. I thank Yihsin Tang (Chris) for his assistance and encourage. And I also thank all people who help me during the lifetime. Life in Western is pleasant and excited. And I hope I can stay here for a while.

Ye Luo

TABLE OF CONTENTS

ACKNOWLEDGEMENTS.....	ii
LIST OF FIGURES.....	iv
1. Introduction	1
2. Theoretical Support.....	3
2.1. Lattice Boltzmann method	3
2.2. Immersed-boundary lattice Boltzmann method.....	4
2.3. Generalized lattice spring model.....	6
2.4. lattice Boltzmann flexible particle method	7
3. Simulation Set-up.....	9
3.1. Single swimming body.....	9
3.2. Two-body system	10
4. Results and Discussion	12
4.1. Single swimming body.....	12
4.1.1. Propulsive performances quantification	12
4.1.2. Effects of flexibility on periodic V_y , V_z , C_d and C_p	13
4.1.3. Effects of flexibility on U_c , C_p and η	18
4.1.4. Flexibility effects on turning point.....	21
4.1.5. Resonance	22
4.1.6. Effects of flexibility on flapping amplitude and mode shape	23
4.2. Two swimming bodies in tandem configuration	28
4.2.1. Equilibrium of separation distance.....	28
4.2.2. Flow field analyses	29
5. Conclusions	32
REFERENCES.....	34

LIST OF FIGURES

1 D3Q15 lattice model.....	4
2 Fluid and solid particles in IB-LBM	6
3 The illustration of GLSM	7
4 Simulation set-up for single swimming body	9
5 Simulation set-up for tandem configuration	11
6 Effects of flexibility on forward velocity.....	15
7 Effects of flexibility on undulation velocity	16
8 Effects of flexibility on drag force	17
9 Effects of flexibility on power coefficient.....	18
10 Normalized cruising speed as a function of rigidity El.....	19
11 Power coefficient as a function of rigidity El.....	20
12 Propulsive efficiency as a function of rigidity El.....	21
13 Migration against time steps.....	22
14 a) The evolution of normalized cruising speed with increasing reduced frequency; b) The evolution of power coefficient with increasing reduced frequency	23
15 The flapping mode shape and the graph of V_z against Z/L (cases $Re=5$).....	25
16 The flapping pattern for one period (case $Re=75$).. ..	26
17 The flapping pattern for one period (case $Re=100$).. ..	27
18 Separation distance as a function of time.....	29
19 The fluid flow figure for cases with phase difference.....	29
20 The fluid flow figure for cases without phase difference.....	30

1. Introduction

Our world is filled with swimming bodies. The research of simulation of swimmers is one of the most important branches among the field of biophysics. It is a comprehensive research area with biologists, mathematicians, chemists, pharmacologists and engineers of chemical, biotechnology, etc engaged on. The simulation of microorganism swimmers is applied widely in the area of medicine, pharmacology, environment treatment, biotechnology and chemical engineering.

In 1951, Taylor (1951)[2] firstly explained how microorganisms could propel itself using the viscous force and set up the theoretical mathematic model. In 1958, the locomotion pattern of flagella-like swimmer was calculated by Machin (1958)[3]. In 1977, Purcell (1977)[4] introduced the general “scallop theorem” to provide more inside calculations about flagella-like motions. The Scallop theorem states that to achieve propulsion at low Reynolds number in Newtonian fluids a swimmer must deform in a way that is not invariant under time-reversal. In 1998, Wiggins et al.(1998)[5][6] introduced a new theory, elastohydrodynamics, to compared with the experimental results and obtained good agreement between theory and experiment. Since then, elastohydrodynamics played a significant role in the field of microorganism swimmers simulation due to predicting the shape pattern and the propulsive force of flagella in fluid successfully.

In addition to the theory development, the experimental observations of microorganism swimmers were also preferred elsewhere, such as Wiggins & Goldstein (1998)[6] observed the shape pattern and then they proposed the bending modul for the flagella; Yu et al. (2006)[7] measured the propulsive force of the swimming flagella; Pak et al. (2011)[8] designed a flexible nanowire motor to give high-speed propulsion for the flagella; Lagomarsino and Lowe et al. (2003)[9] used the slender body theory to simulate the flagellum locomotion and Eric & Powers (2009)[10] summarized theoretical and experimental studies for the hydrodynamics

of swimming microorganisms.

However, generally the simulations are based on models that similar to real swimmers while the methods of simulations are presented seldom. In this project, a numerical experimental method which combines generalized lattice spring model (GLSM) and the immersed-boundary lattice Boltzmann method (IBLBM) will be applied.

Moreover, the study of swimming body means much wider field of computer simulation --- not only the microorganism swimmers, but also all flapping swimming motion. So it is important to found a generalization of swimming bodies.

Before this study, seldom articles focus on undulation flapping in three dimension flow distribution at high Reynolds number. Some researches establish a flow field in three dimensions while fail to perform a high Reynolds Number case.[11] Some researches only succeed in 2-D flow field.[12] And also, lots of them employed the traditional computational fluid dynamics methods (CFD) for fluid simulation. Comparing to Lattice Boltzmann method which we use in this study, traditional method has simpler governing equations but more difficulty for coding program.

Two-body system is also studied in this research and results are reported and compared with previous study in 2-D flow field by traditional method.[13] Detailed information will be given in the section of simulation set-up.

2.Theoretical Support

2.1. Lattice Boltzmann method

Lattice Boltzmann Method is a relatively new simulation technique for complex fluid systems and has several advantages over other conventional computational fluid dynamics methods. Instead of solving the Navier–Stokes equations, the discrete Boltzmann equation is solved to simulate the flow of a Newtonian fluid with collision models such as Bhatnagar-Gross-Krook (BGK).

In LBM, a group of lattice nodes are used to represent fluid. Each node has distribution functions f and discrete velocity \mathbf{e}_σ is the order number of direction which depends on different models and will be discussed in later section. The Boltzmann equation with BGK single relaxation time is

$$f_\sigma(\mathbf{r} + \mathbf{e}_\sigma, t + 1) = f_\sigma(\mathbf{r}, t) - \frac{1}{\tau} [f_\sigma(\mathbf{r}, t) - f_\sigma^{eq}(\mathbf{r}, t)]$$

where $f_\sigma^{eq}(\mathbf{r}, t)$ is the equilibrium distribution function at position \mathbf{r} and time t

$$f_\sigma^{eq} = \omega_\sigma \rho_f \left\{ 1 + 3(\mathbf{e}_\sigma \cdot \mathbf{u}) + \frac{2}{9}(\mathbf{e}_\sigma \cdot \mathbf{u})^2 - \frac{3}{2}(\mathbf{u} \cdot \mathbf{u}) \right\}$$

The macroscopic fluid density ρ_f and the momentum density are given as

$$\rho_f = \sum_{\sigma} f_\sigma$$
$$\rho_f \mathbf{u} = \sum_{\sigma} f_\sigma \mathbf{e}_\sigma$$

Lattice Boltzmann models can be operated on a number of different lattices, both cubic and triangular, and with or without rest particles in the discrete distribution function.

In this study, the D3Q15 lattice model is employed. Here "D3" stands for "3 dimensions" and "Q15" stands for "15 nodes". Figure 1 shows illustration of D3Q15 model.

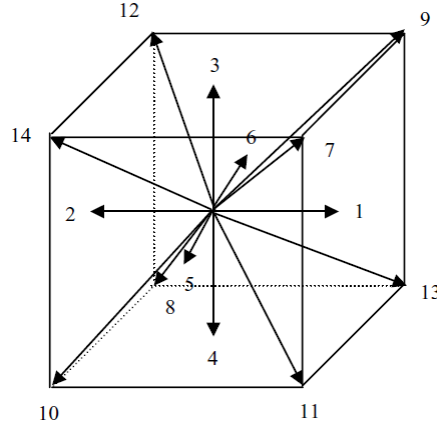


Figure 1 D3Q15 lattice model

In this model, the lattice velocities are defined as

$$e_{\sigma} = \begin{cases} (0,0,0) & \sigma = 0 \\ (\pm 1, 0, 0), (0, \pm 1, 0), (0, 0, \pm 1) & \sigma = 1 \\ (\pm 1, \pm 1, \pm 1) & \sigma = 2 \end{cases}$$

and the weight coefficients are given by

$$\omega_{\sigma} = \begin{cases} 2/9 & \sigma = 0 \\ 1/9 & \sigma = 1 \\ 1/72 & \sigma = 2 \end{cases}$$

and the kinematic viscosity is related to the relaxation time

$$\nu = \frac{1}{3} \left(\tau - \frac{1}{2} \right)$$

2.2. Immersed-boundary lattice Boltzmann method

Immersed-boundary lattice Boltzmann method (IBLBM) is a numerical method which combines the lattice Boltzmann method and the immersed-boundary method (IBM). The IBM coupled with LBM was presented by Feng & Michaelides (2004) [14] and Wu & Aidun (2010) [15]. IBM solves the fluid-solid interaction problem.

In IBM, fluid nodes are applied to a regular Eulerian grid, so every boundary solid node will not coincide with the exactly adjacent fluid node. Then, the fluid velocity at the boundary solid node can be derived from the fluid velocity of the surrounding fluid nodes, which is given as the discrete Dirac Delta function (Peskin, 2002) [16]

$$D(\mathbf{r}) = \begin{cases} \frac{1}{64h^3} \left(1 + \cos \frac{\pi x}{2h}\right) \left(1 + \cos \frac{\pi y}{2h}\right) \left(1 + \cos \frac{\pi z}{2h}\right) & |\mathbf{r}| \leq 2h \\ 0 & |\mathbf{r}| > 2h \end{cases}$$

where h is the lattice length. The fluid velocity \mathbf{u}_f at the position of the solid boundary node is given by

$$\mathbf{u}_f(\mathbf{r}^b, t) = \int_{\Pi} \mathbf{u}(\mathbf{r}^l, t) \mathcal{D}(\mathbf{r}^l - \mathbf{r}^b) d\mathbf{r}^l$$

where Π and $2h$ mean that fluid nodes are within a spherical volume Π of a radius of $2h$, centered at a given solid node. \mathbf{r}^b is the boundary solid position and \mathbf{r}^l is the position of the lattice fluid nodes within the sphere as shown in Figure 2. The small circles represent fluid particles and the blue small squares represent solid particles; large circles represent spheres around their central solid particle; squares with the thicker edges are the boundary solid particles which directly interact with their surrounding fluid particles within a sphere. For instance, as in Figure 2 b), step 1 shows that the flow velocities of fluid particles $\mathbf{u}(\mathbf{r}^l, t)$ are interpolated to their central the k^{th} solid particle and step 2 shows that the reaction force of the k^{th} boundary solid particle on the fluid is interpolated to the surrounding fluid particles. The arrows denote the direction of interpolation in step 1 and step 2. Under the condition without slipping, the boundary solid node velocity $\mathbf{u}_s(\mathbf{r}^b, t - 1)$ is equal to the fluid node velocity $\mathbf{u}_f(\mathbf{r}^b, t)$, and thus the difference of velocities represents the interaction force \mathbf{F}^{int} on the solid boundary over one time step as

$$\mathbf{F}^{\text{int}}(\mathbf{r}^b, t) = \rho_f(\mathbf{u}_f(\mathbf{r}^b, t) - \mathbf{u}_s(\mathbf{r}^b, t - 1))$$

Then the discrete Dirac delta function is employed again to distribute the reaction force to the surrounding fluid nodes

$$\mathbf{g}(\mathbf{r}^l, t) = - \int_{\Gamma} \mathbf{F}^{\text{int}}(\mathbf{r}^b, t) \mathcal{D}(\mathbf{r}^l - \mathbf{r}^b) d\mathbf{r}^b$$

where $\mathbf{g}(\mathbf{r}^l, t)$ is the distributed reaction force and Γ is a spherical volume of a radius of $2h$, located at \mathbf{r}^l . Force distribution process is illustrated in step 2 of Figure 2 b).

Finally, the reaction force term is added to the Boltzmann equation as

$$f_{\sigma}(\mathbf{r} + \mathbf{e}_{\sigma}, t + 1) = f_{\sigma}(\mathbf{r}, t) - \frac{1}{\tau} [f_{\sigma}(\mathbf{r}, t) - f_{\sigma}^{eq}(\mathbf{r}, t)] + 3\omega_{\sigma}(\mathbf{g} \cdot \mathbf{e}_{\sigma})$$

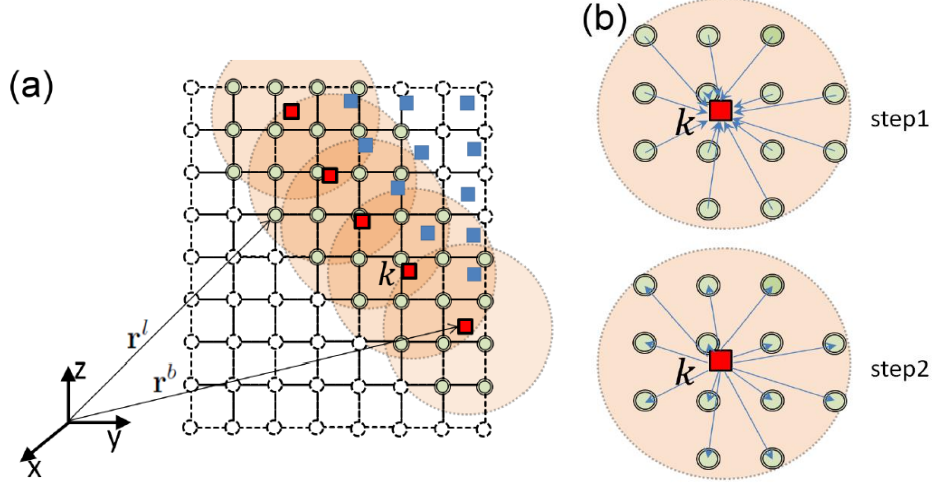


Figure 2 Fluid and solid particles in IB-LBM, and two steps of velocity and force interpolation

2.3. Generalized lattice spring model

In microscopic space, the intermolecular force can be regarded as to conform to the Hooke's law. Based on this idea, the concept of lattice spring model (LSM) is provided by Buxton et al. (2005)[17] to simulate the elastic structure. The model includes two core parts: 1) Mass nodes space regularly initially; 2) Two adjacent nodes are linked by harmonic springs. In this way, the spring energy U_i^s acted on the i^{th} node is given by

$$U_i^s = \frac{1}{2} k_s \sum_j (\mathbf{r}_{ij} - \mathbf{r}_{0ij})^2$$

where k_s is the spring coefficient; \mathbf{r}_{0ij} is the equilibrium length of the spring between two neighboring particle i and j ; j is the nearest neighboring solid particle of the i^{th} solid particle; and $\mathbf{r}_{ij} = \mathbf{r}_i - \mathbf{r}_j$. The spring force is a two body central force which allows either extension or compression between two solid particles. However, this kind of spring force cannot handle bending deformation precisely; the generalized lattice-spring model (GLMS) will be introduced to describe an additional three body force among solid particles. The angular energy U_i^a is shown as

$$U_i^a = \frac{1}{2} k_a \sum_j \sum_{k, k \neq j} (\theta_{ijk} - \theta_{0ijk})^2$$

where k_a is the angular coefficient; j and k are the nearest neighboring solid particles of i^{th} solid particle; θ_{ijk} is the angle between the bonding vectors \mathbf{r}_{ij} and the bonding vector \mathbf{r}_{ik} ; θ_{0ijk} is the corresponding equilibrium angle. Then the elastic force F_i on the i^{th} solid particle can be computed from the gradient of the total energy.

$$\mathbf{F}_i = -\nabla(U_i^s + U_i^a)$$

If the solid structure is isotropic, the elastic modulus of the solid body can be related to the spring and angular coefficients by

$$E = \frac{k_s}{r_0}$$

$$G \approx \frac{4k_a}{r_0^2}$$

where E is the Young's modulus of the deformable solid body and G is its shear modulus. The derivation of the relationship between k_s and E and the relationship between k_a and G is presented in Wu's article (2014) [1]. Then the total force drives the movement of solid particles

$$\mathbf{F}_T^i = \mathbf{F}_i + \mathbf{F}^{int}$$

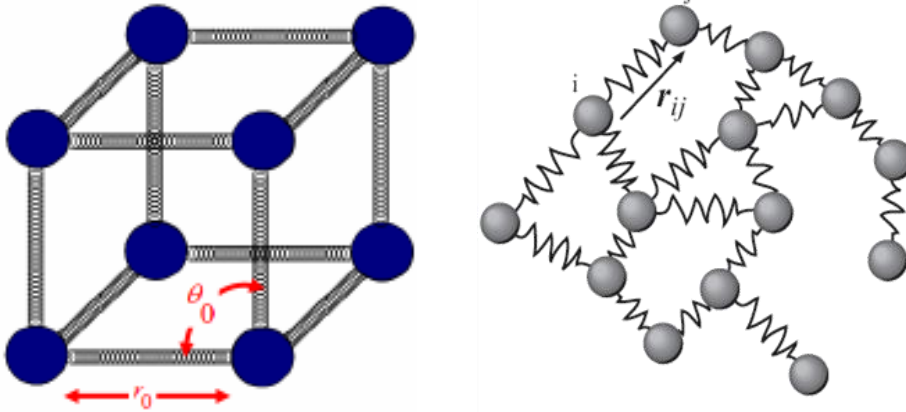


Figure 3 The illustration of GLSM

2.4. lattice Boltzmann flexible particle method

Another numerical simulation method, the lattice Boltzmann flexible particle method(LBFPM), has been successfully used to simulate fluid-structure interactions

by Qi et al.(2010)[**18**] and Liu et al. (2011)[**19**].

A flapping of a flexible swimming body in fluid flows at a given Reynolds number will be simulated by the present method and the results will be compared with those by using the Lattice Boltzmann flexible particle method.

3.Simulation Set-up

3.1. Single swimming body

Essentially, this research studies the locomotion patterns of solid swimming bodies in 3-D lattice Boltzmann flow field. In detailed, a self-propelled swimming body is driven by the vertical oscillation, and the simulation is performed in a 3-D fluid box.

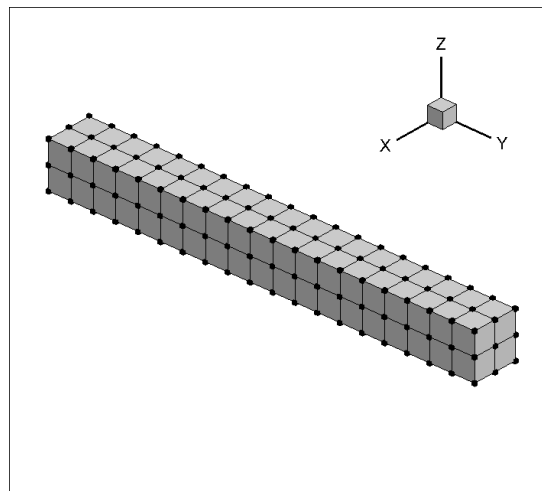


Figure 4 Simulation set-up for single swimming body

At the initial time, the solid swimming body is set up in the center of the whole flow field. For the structure of swimmer itself, as shown in Fig.5, the swimming body is constituted by 180 solid particles which are linked each other by spring model. The 180 particles combine and form a rectangular cuboid sizing $3 \times 3 \times 20$ respectively corresponding to X, Z and Y directions. The length of the solid body is along with Y direction in which we regard as migration direction. The vertical oscillation is set up in the Z direction. Since X direction has no contribution to the flapping or migration, in this article, any tiny motion in X direction will be ignored.

Corresponding to setting of three directions, fluid flow box is set up as a rectangular box of sizes [0 30], [0 300], [0 90] in X, Y and Z direction. And digits mean fluid nodes in LBM. The periodic boundary is introduced to eliminate influence of boundary. Then the flow field can be regarded as infinite in a sence.

The flapping pattern is deducted from equations of harmonic motion, shown as

below

$$Z(t) = \bar{A}\sin\omega t$$

where z stands for the direction of swing of swimming body; z_0 is the amplitude; ω is the flapping angular frequency and t is time. This equation forces each particle which combines the whole swimming solid part to the particular place and then mimic the real swimming body. Then the maximum of velocity of driven point can be described as

$$V_z^{max} = \bar{A}\omega$$

To investigate the performance of cases with different physical quantities, such as Reynolds number, dimensionless bending rigidity, size of swimming body, separation distance and etc., one parameter is varied while keeping others fixed. Through the studying of subsequent locomotion patterns, we validate success of this research.

Among different kinds of physical variables which effects on the propulsive performance, the flexibility of swimming body is a key influencing factor. In this study, three kinds of cases are chosen for one case at low Reynolds number and two cases at high Reynolds number. Table 1 shows basic input settings for every case.

Table 1 Basic input setting of cases with different Reynolds number

	Re	\bar{A}	$f(\text{Hz})$	ρ_s	ρ_f	μ_f
Case A	5	9.0	0.679775	1.0	1.0	0.16
Case B	75	9.0	10.196568	1.0	1.0	0.01
Case C	100	9.0	13.867332	1.0	1.0	0.01

where Re is Reynolds number, \bar{A} is amplitude, f is flapping frequency, ρ_s is solid density, ρ_f is fluid density and μ_f is fluid viscosity. All parameters listed above are in LBM units excepting flapping frequency.

3.2. Two-body system

Two-body system simulation begins with the initial setup of a tandem configuration as figure 5. For each fiber, the setup is exactly same as that of single fiber. In this research, we find the optimum solid rigidity in single fiber section and

then introduce to two-body tandem system. The separation distance is known as the distance between center mass of front and rear swimming bodies. It will be evolved along with time period and is the key result for this research. The cases are listed in

Table 2 Basic input setting of cases with 0° and 90° phase difference

	Re	EI	$\Delta\phi$	D_{yi}
Case A	75	0.016	0°	a)1.5 b)2 c)2.5 d)3
Case B	75	0.016	90°	a)1.5 b)2.2 c)2.6 d)3 e)4

where term $\Delta\phi$ is phase difference. D_{yi} is the initial separation distance.

Since all length are normalized by the length of swimming body (which in this study is 20). It is easy to derive that when $D_{yi} = 1$, two swimming bodies are in contact.

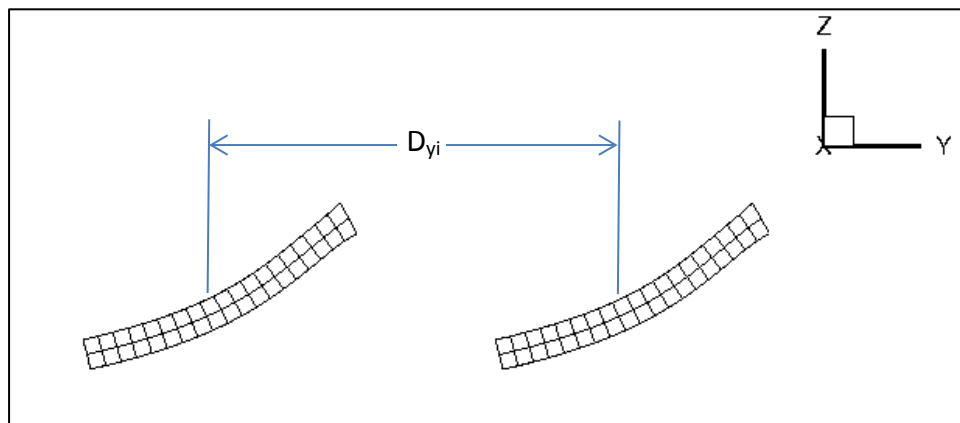


Figure 5 Simulation set-up for tandem configuration

4. Results and Discussion

4.1. Single swimming body

4.1.1. Propulsive performances quantification

To quantify the propulsive performance, some physical parameters are introduced as follows. First, the migration of center mass functioning of time period can visually illustrate the locomotion of swimming body. In this study, since Y direction is set up as the migration direction, migration function is as

$$\frac{Y}{L} = f(t)$$

where Y/L means normalized location in which L is the length of swimming body and t is the time period in keeping with flapping undulation cycle.

Second, the Y-velocity V_y is defined as the average velocity of every solid particle in direction of migration at each time period,

$$V_y = -\frac{1}{180} \int_1^{180} (v_y) ds$$

where v_y is velocity of each particle in Y direction and s is index of solid particles. All velocity mentioned in this study is normalized by the maximum velocity in Z direction.

Then the Z-velocity V_z is defined in the same way, and known as flapping velocity,

$$V_z = -\frac{1}{180} \int_1^{180} (v_z) ds$$

And cruising speed U_c is defined as the average migration velocity of swimming body after reaching steady state (absence of acceleration).

$$U_c = -\frac{1}{\Delta t} \int_{t_1}^{t_2} (V_y) dt$$

Third, drag coefficient C_d for each time step is collected from combining all

fluid-on-particles force in Z direction. It is the force calculated by second order derivation of migration in essence.

$$C_d = -\frac{1}{180} \int_1^{180} \left(\frac{\partial^2 Z}{\partial t^2} \right) ds$$

Power coefficient C_p is defined in another way. It is employed to measure the average output power required to produce the forward migration of solid swimming bodies. It can be integral as

$$C_p = -\int_0^{180} \left(\frac{\partial^2 Y}{\partial t^2} \right) \left(\frac{\partial Y}{\partial t} \right) ds$$

In essence, power coefficient is the product of that velocity times force. And the average power coefficient in section 4.1.3 is calculated after reaching steady state.

Then, propulsive efficiency η is simply defined as

$$\eta = \frac{U_c}{C_p}$$

At last, for describing the physical properties of solid swimming body, rigidity EI and Reynold number Re are introduced and defined as follows

$$EI = \frac{\pi E r_a r_b^3}{3l_b}$$

$$Re = \frac{\bar{A}\omega L}{\mu_f}$$

where E is Young's modulus, r_a and r_b are half of width and height of the swimming body, l_b is bond length which is 1 in simulation units, \bar{A} is flapping amplitude, ω is angular frequency of flapping undulation, L is length of the swimming body and μ_f is fluid viscosity. All parameters should be converted from simulation units of input data to real units by unit factors.

4.1.2. Effects of flexibility on periodic V_y , V_z , C_d and C_p

Periodic graphs directly indicate the flapping locomotion pattern of swimming body in one period after reaching steady state.

Since the migration of swimming body only occurs in Y direction, average

velocity in this direction is introduced to stand for forward velocity V_y . Fig.7 shows effects of flexibility on forward velocity for all cases in this research. For each time step, velocity is calculated by averaging every solid particle's velocity at this moment. The velocity of each particle is added by two parts, the undulate deformation of swimming body and the cruising speed. The swimmer moves forward or backward uniformly, so the flapping of swimming body causes the undulation. Graphs a) and b) in Figure 6 suggest along with the increasing rigidity, both the relative position and undulate range of forward velocity increase while graphs c)&d) and e)&f) in Figure 6 shows a trend of increasing before a maximum and decreasing then. In other words, Either at low or high Reynolds number, a maximum seems existing along with the changing rigidity. Actually, these phenomena match with the evolution of cruising speed on rigidity very well and will be discussed in next section.

Average velocity of all solid particles in Z direction is introduced as flapping velocity V_z . The patterns of flapping velocity are similar to each other for all cases with low or high Reynolds Number (see figure 7). The whole trend is that for the case of higher cruising speed, the amplitude of the flapping velocity is higher. This connection is obvious that larger range of flapping results into higher propelling and then, higher forward speed. It will be discussed in the section of mode shape at full length.

Drag coefficient C_d for each printed time step is collected from combining all fluid-on-particles force in Z direction. For cases with same Reynolds number, the periodic patterns are similar to each other (see figure 8). The amplitude of drag coefficient is in keeping with amplitude of flapping velocity because both of them describe undulation of flapping essentially.

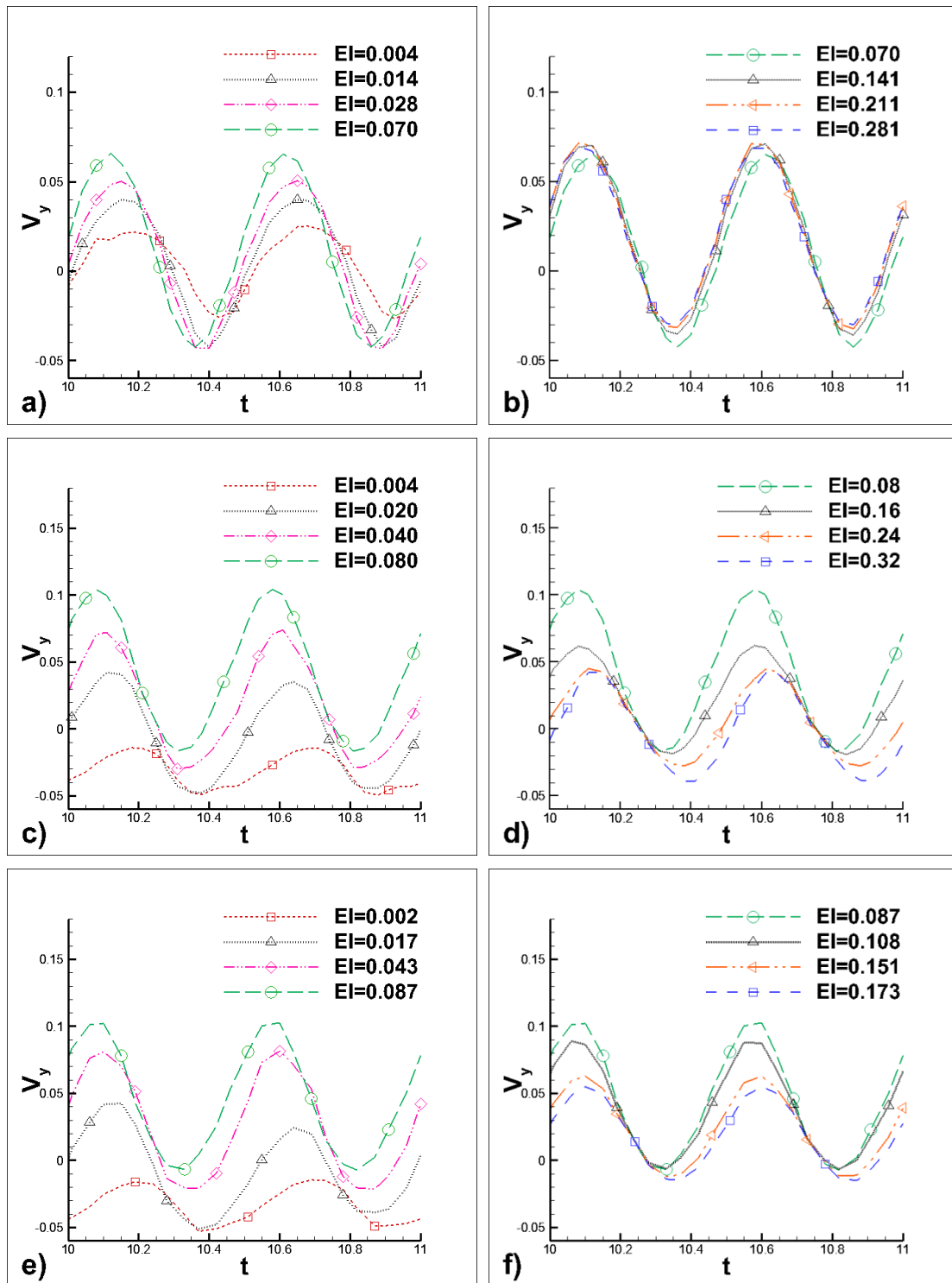


Figure 6 Effects of flexibility on forward velocity.

figure a) and b) corresponds to case of $Re = 5$, which is case A in Table 1, figure c) and d) to case B of $Re = 75$, and figure e) and f) to case C of $Re = 100$. Same cases corresponding in figure 8, figure 9 and figure 10.

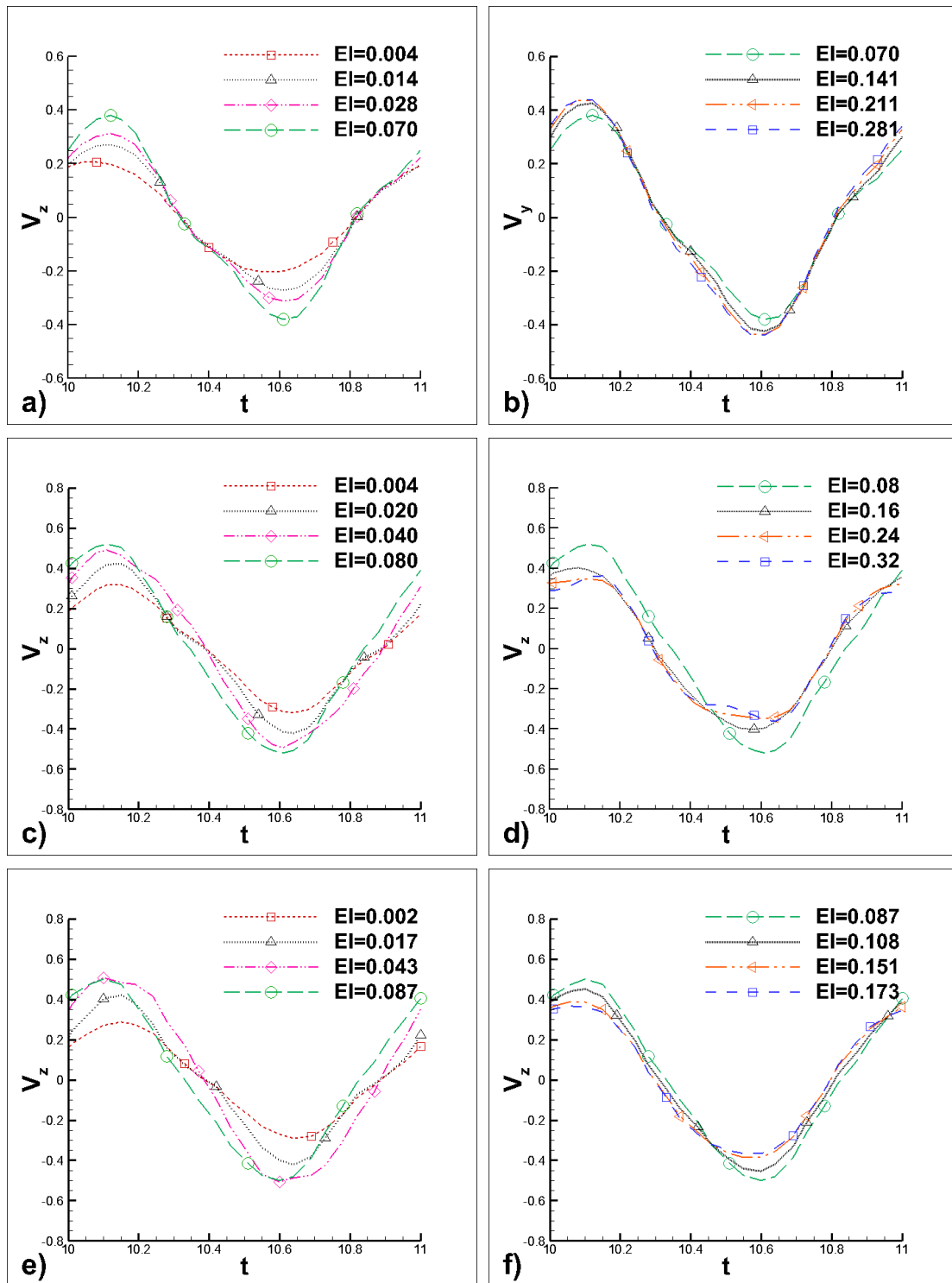


Figure 7 Effects of flexibility on undulation velocity

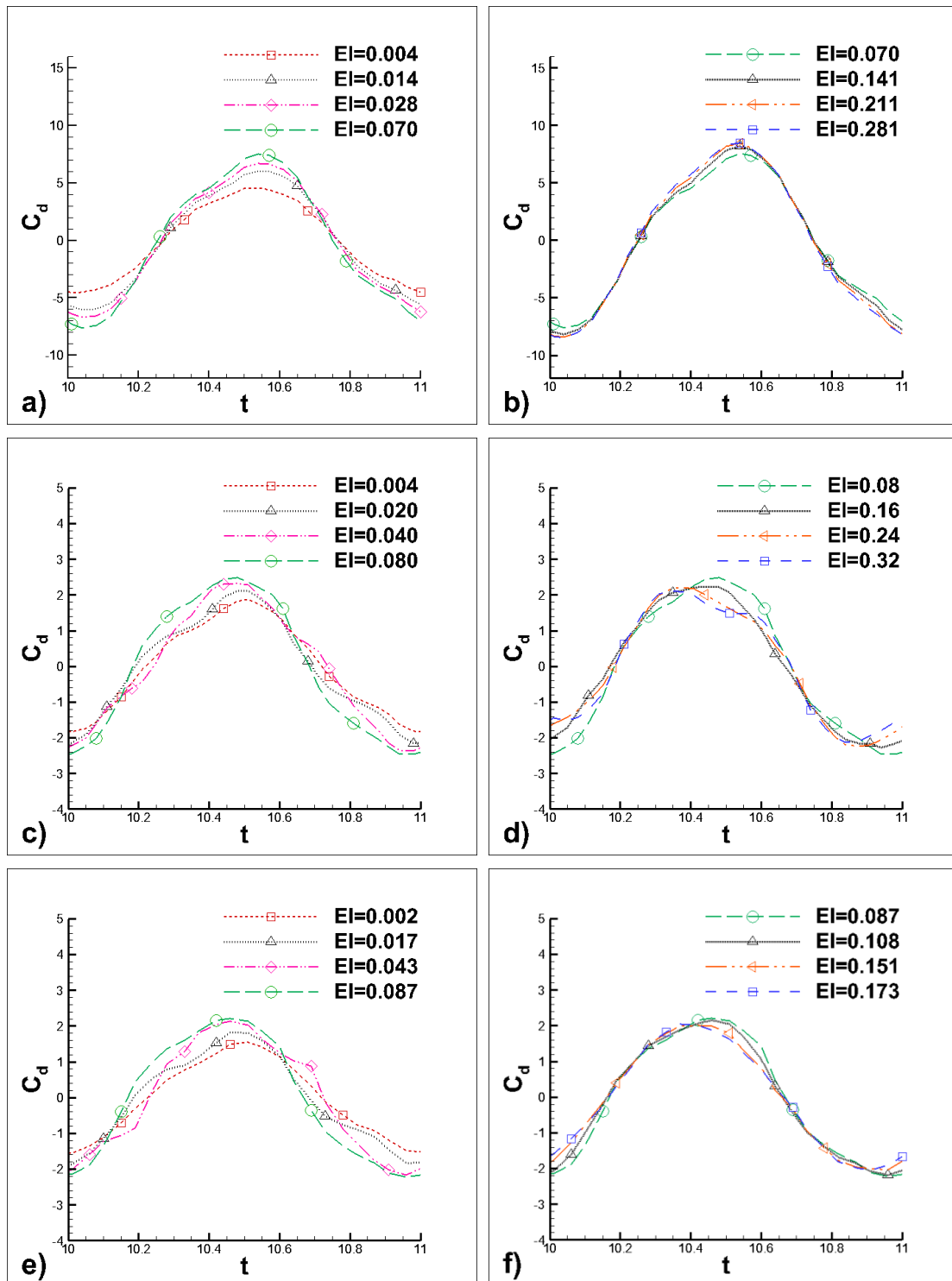


Figure 8 Effects of flexibility on drug force

The periodic changing of power coefficient in one cycle has the same trend with forward velocity. Figure 9 also shows a possibility of maximum of forward power which is confirmed and fully discussed in next section.

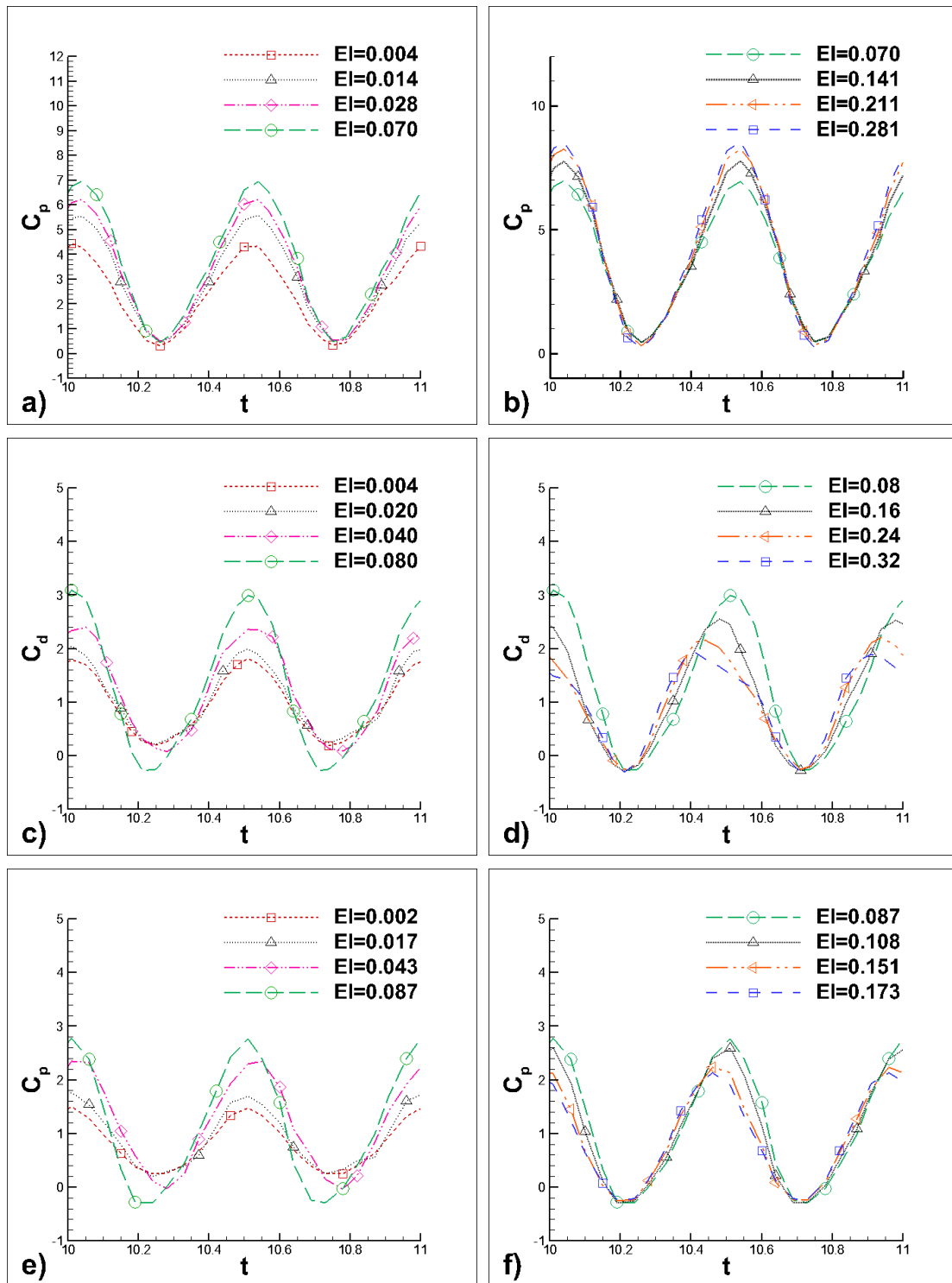


Figure 9 Effects of flexibility on power coefficient

4.1.3 Effects of flexibility on U_c , C_p and η

The evolution of normalized cruising speed along with the increasing flexibility known as EI is shown in the Figure 10. And for each case in the figure, the

parameters are listed in the Table 1 as the reference. Essentially, for the cases A, B and C, we change the flapping frequency f to gain given Reynolds Number. In case A, the fluid viscosity is also changed to keep the period steps of swimmers.

The overall trend in all cases in figure 10 shows a global maximum will be achieved at a point which can be regarded as an optimal point. Some similar results of the cruising speed depending on rigidity were also reported in the Zhu's article which focused on the 2-D flow area (Zhu, X., 2014) [12] and Lee's article at low Reynolds Number (Lee, J., 2013) [20]. Unfortunately, being limited to the mathematic model of Lattice Boltzmann Method which we employed, it is hard to run cases with normalized Young's modulus higher than 0.82. Besides, local maximum of cruising speed is also found in case B.

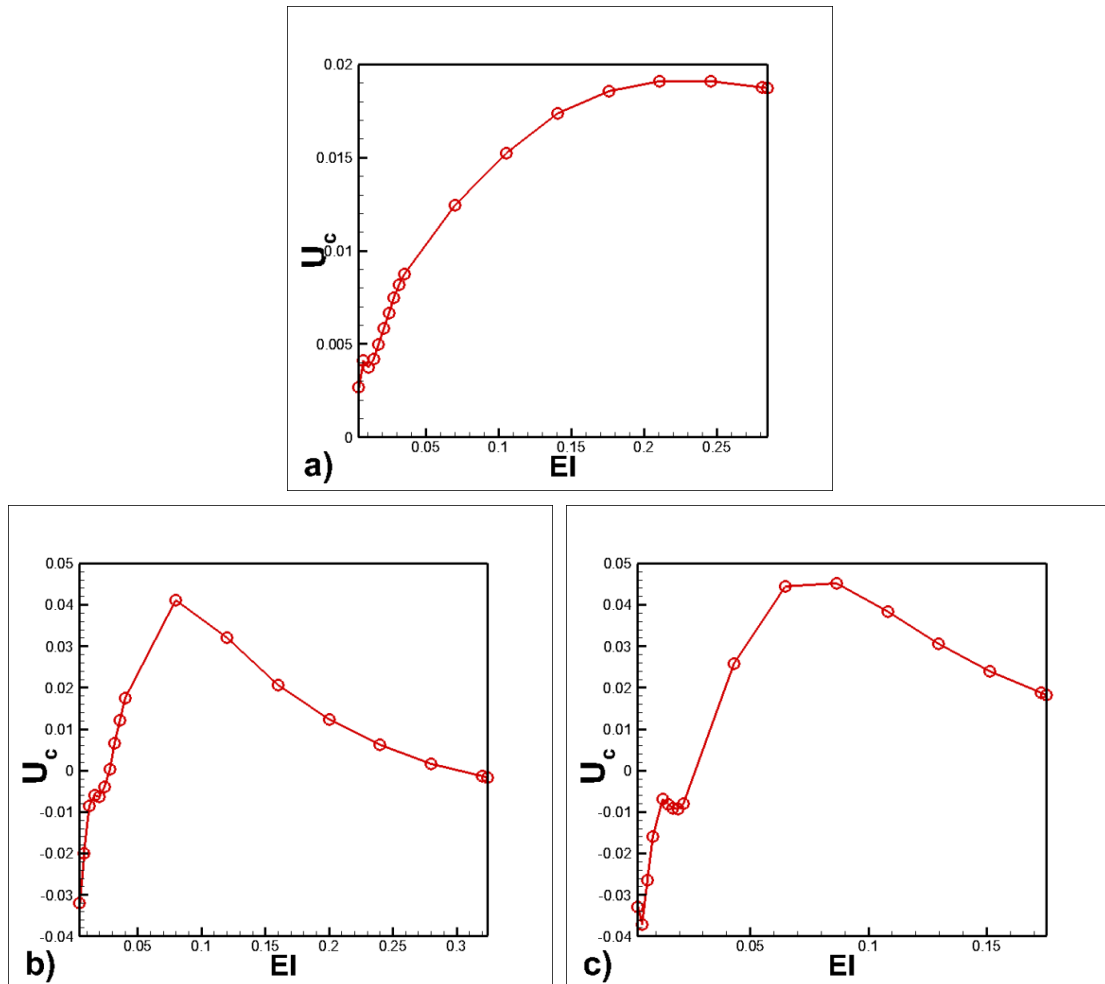


Figure 10 Normalized cruising speed as a function of rigidity EI .
a)case A, b)case B and c) case C in Table 1.

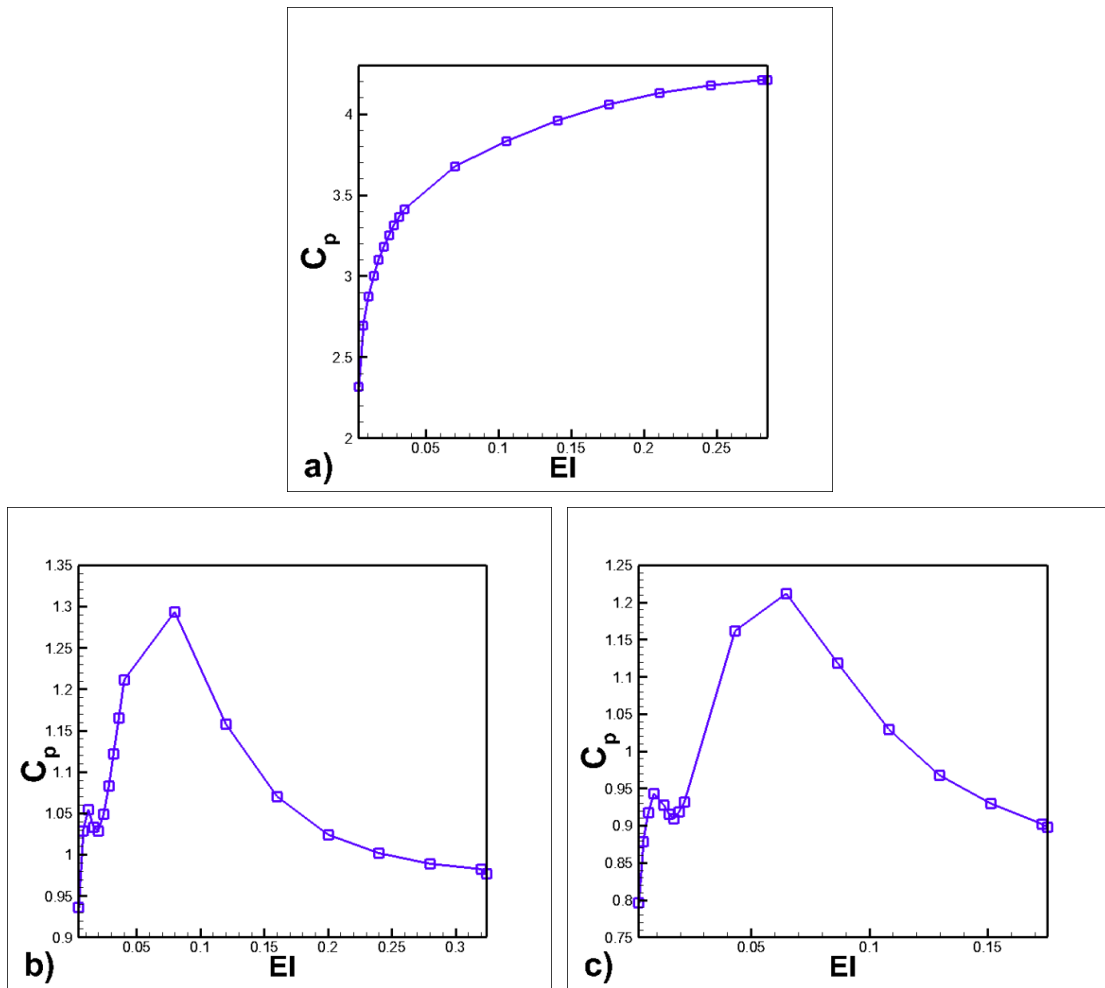


Figure 11 Power coefficient as a function of rigidity EI .

a)case A, b)case B and c) case C.

For all cases, the graphs of power against EI (see figure 11) have the similar curve comparing to the graphs of speed against EI . This is very simple to understand that higher propulsive force results into fast forward migration. However, because of different efficiency for changing rigidity, the graph of C_p and U_c are not selfsame. Case C as an example, the rigidity around $EI = 0.15$, lower C_p leading to higher U_c contrasts with rigidity of $EI = 0.02$ in which same C_p leading to a negative U_c .

The propulsive efficiency is the quotient by U_c/C_p . Due to the small changing of power coefficient, the graph of efficiency (see figure 12) has similar evolution with graph of cruising speed. From the original data, for all cases in this study, rigidity which leads to maximum of cruising speed also leads to maximum of efficiency. In the cases with $Re=100$, case of $EI=0.065$ and case of $EI=0.087$ have very similar cruising speed but different power coefficient, and then maximum of efficiency

occurs for $EI=0.087$. Thus, it is preferred to consider the case with maximum efficiency as optimal point. For all graphs in this section, same trends are also reported in [12].

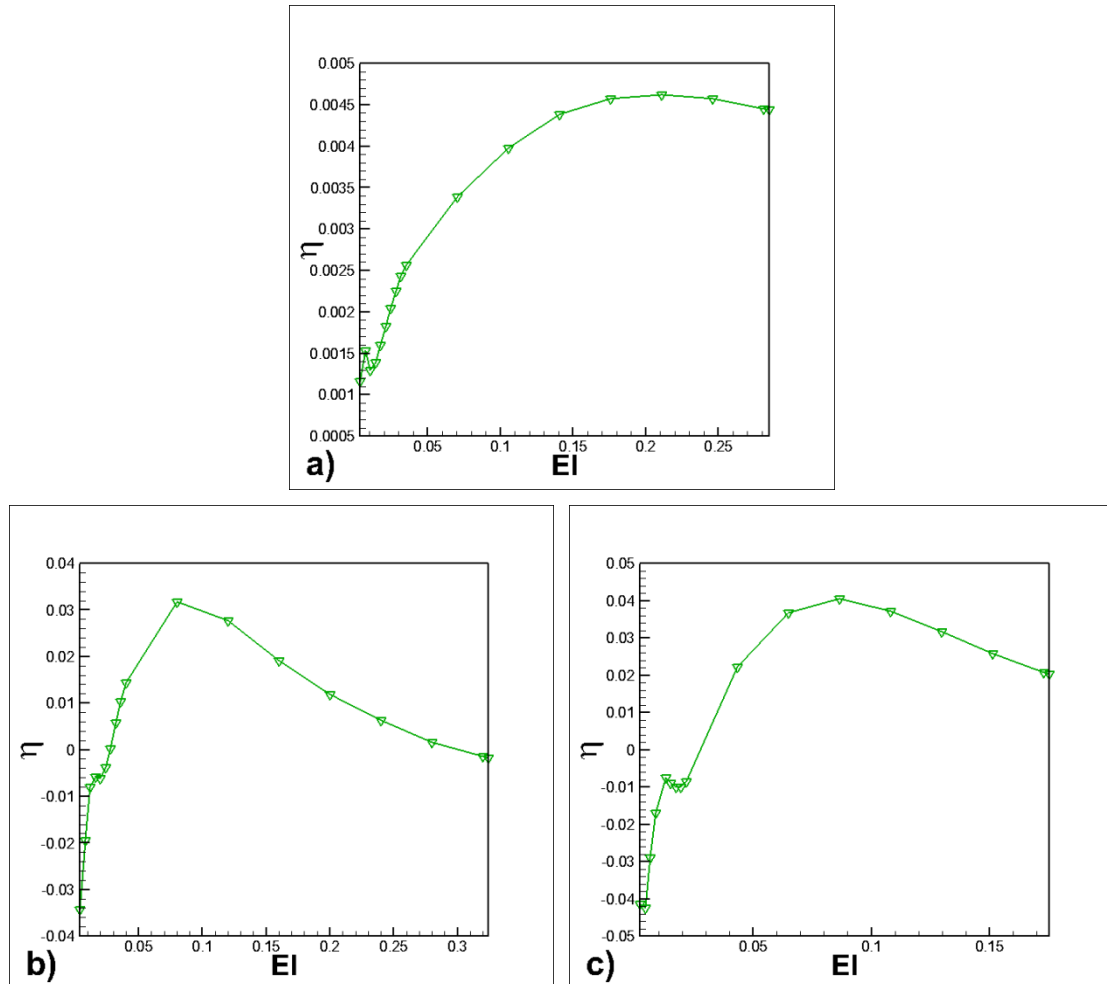


Figure 12 Propulsive efficiency as a function of rigidity EI .
a)case A, b)case B and c) case C.

4.1.4 Flexibility effects on turning point

For a direct view of locomotion, the migration of center mass of single swimming body is shown to illustrate direction and vibration. Figure 13 is the graph of migration against time steps. This section focuses on the turning point of rigidity where the solid body travels from backward to forward. Figure 10 is as a reference.

To most cases in our study, solid bodies swim forward, along with the positive Y direction. While to cases with high Reynolds number and low rigidity, the swimmers may move backward (see figure 10). The mechanism of forward migration driven by

flapping is simple. As in all self-propelling systems, the propulsion of a swimming body depends on the fact that the retarding effect of all the tangential force acting along the body is compensated by propulsive components of force acting normally to the surface of the body (Gray, 1953) [21]. The backward motion in a self-propelled flapping system has also been reported previously in [12], [22] and [23]. With low rigidity, the mode shape of swimming body (see figure 16 a) and figure 17 a)) is much different with a “standard” flapping mode shape (see figure 16 c) and figure 17 c)). In the mode shape with low rigidity, the “tail” of swimmer forms overbending and pushes fluid forward and then propels itself backward.

However, for cases with low Reynolds number, the high viscosity of fluid restricts the forming of overbending and then backward stage is absent (see figure 10 a) and figure 16 a)).

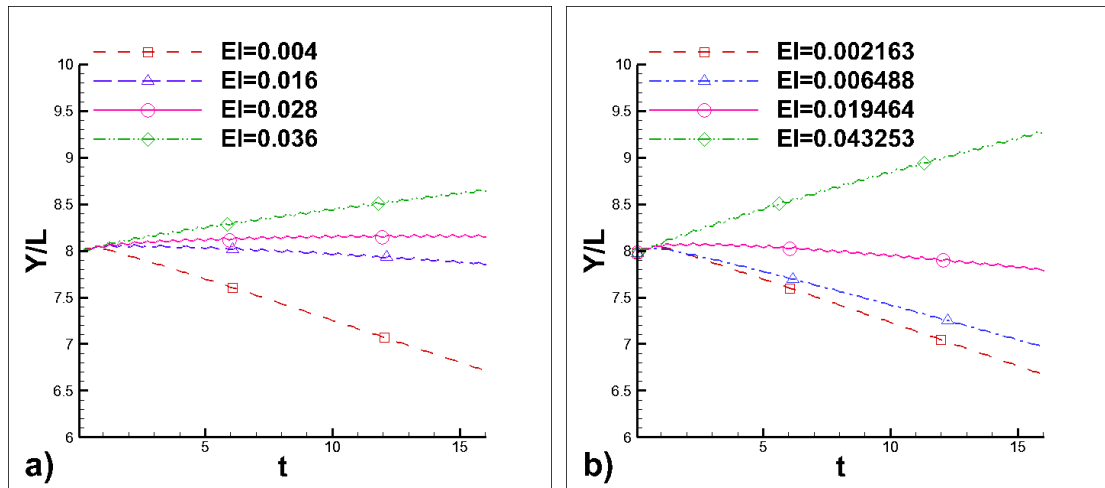


Figure 13 Migration against time steps (initial to 16th time period).
a) case with Re=75 and b) case with Re=100.

4.1.5 Resonance

The role of relation between forcing frequency and natural frequency is very important in optimizing performance. First, the reduced frequency is defined as the ratio between forcing and natural frequency

$$\bar{f} = \frac{f}{f_0}$$

where forcing frequency f is as input frequency and natural frequency f_0 is calculated

by the formula as

$$f_0 = \frac{1}{2\pi} \left(\frac{k_1}{L} \right)^2 \sqrt{\frac{EI}{2\rho_s\rho_f}}$$

where $k_1=1.8751$, L is the length of swimming body, EI is the rigidity, ρ_s is solid density and ρ_f is fluid density. All parameters are in real units and should be converted by the unit factors.

The reduced frequency is employed to quantify resonance. When the forcing frequency equals natural frequency, we consider that resonance occurs in this frequency. The evolution of the normalized cruising speed and power coefficient with increasing reduced frequency is shown in Figure 14 a) and Figure 14 b) respectively.

For cases of high Reynolds number ($Re=75$ or 100), the maxima of U_c and C_p are located in the domain around 1 ($f=0.7-1.3$). The results successfully suggest resonance plays a critical role on flapping, which according with many researches in the field of aerodynamics or fluid dynamics such as [24]. For the cases of low Reynolds number ($Re=5$), there is no obvious maximum in the executable range. However, the original data in this case shows that cruising speed already curves down at the left end.

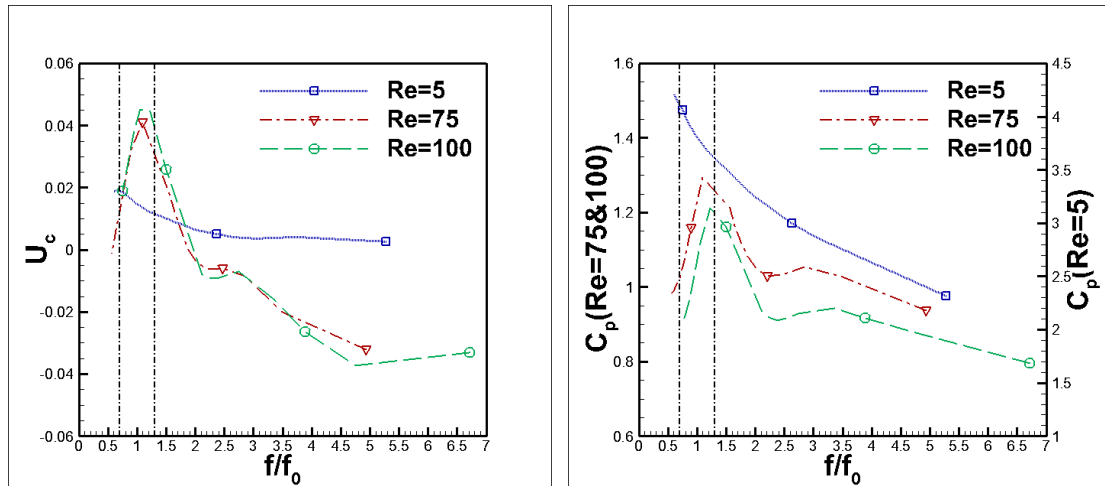


Figure 14 a) The evolution of normalized cruising speed with increasing reduced frequency; b) The evolution of power coefficient with increasing reduced frequency

4.1.6 Effects of flexibility on flapping amplitude and mode shape

In figure 15, four values of flexibility are chosen to note that the former two of

them ($EI=0.035$ & 0.141) result into large range of Cruising speed and later two of them ($EI=0.211$ & 0.281) into similar Cruising speed. In other words, with little differences of domain, the former two obviously have a much larger range than the later two (see fig.). In figure 16, 17, four values sequentially denote backward stage, before-maximum stage, maximum and after-maximum stage (see figure 10).

Since we fix the amplitude of oscillation of swimming body, the locomotion ranges of driven particle in Z direction for all cases are identical. In figure 15, 16 and 17, the right end of swimmers always achieves same coordinates. This fixed amplitude is named as absolute amplitude or set-up amplitude in this article.

At the same time, the average range of swimming body's oscillation is shown in V_z - Z/L graphs in figure 15, 16 and 17. In this coordinate, both V_z and Z/L are harmonic function of time and also have the same frequency. The graph of V_z depending on Z/L forms a closed circle. In this circle, the horizontal diameter is achieved at $V_z = 0$ and can be regarded as the maximal domain of swimmer's center mass. To compare with the absolute amplitude, the term named relative amplitude is employed to indicate this horizontal diameter. In the same way, the vertical diameter which is achieved at $Z/L = 2.25$ is regarded as the maximal range of velocity in flapping direction. With comparing the maximal domain and range, we can quantify the level of mode shape of swimming body.

In figure 15, the area of closed circles largens with the increasing rigidity. Moreover, the changing ratio is completely matching with changing ratio of cruising speed and power efficient. (see figure 11) The first two circles have an obvious difference about the area while the second two circles are almost same. Ignoring the propulsive efficiency, it then suggests that high intensity of flapping leads to faster cruising speed. This is quite in keeping with common sense.

In figure 16 and 17 since existing of clear maxima, closed circles have corresponding maxima in both horizontal and vertical dimensions. Same phenomenon has been reported[12].

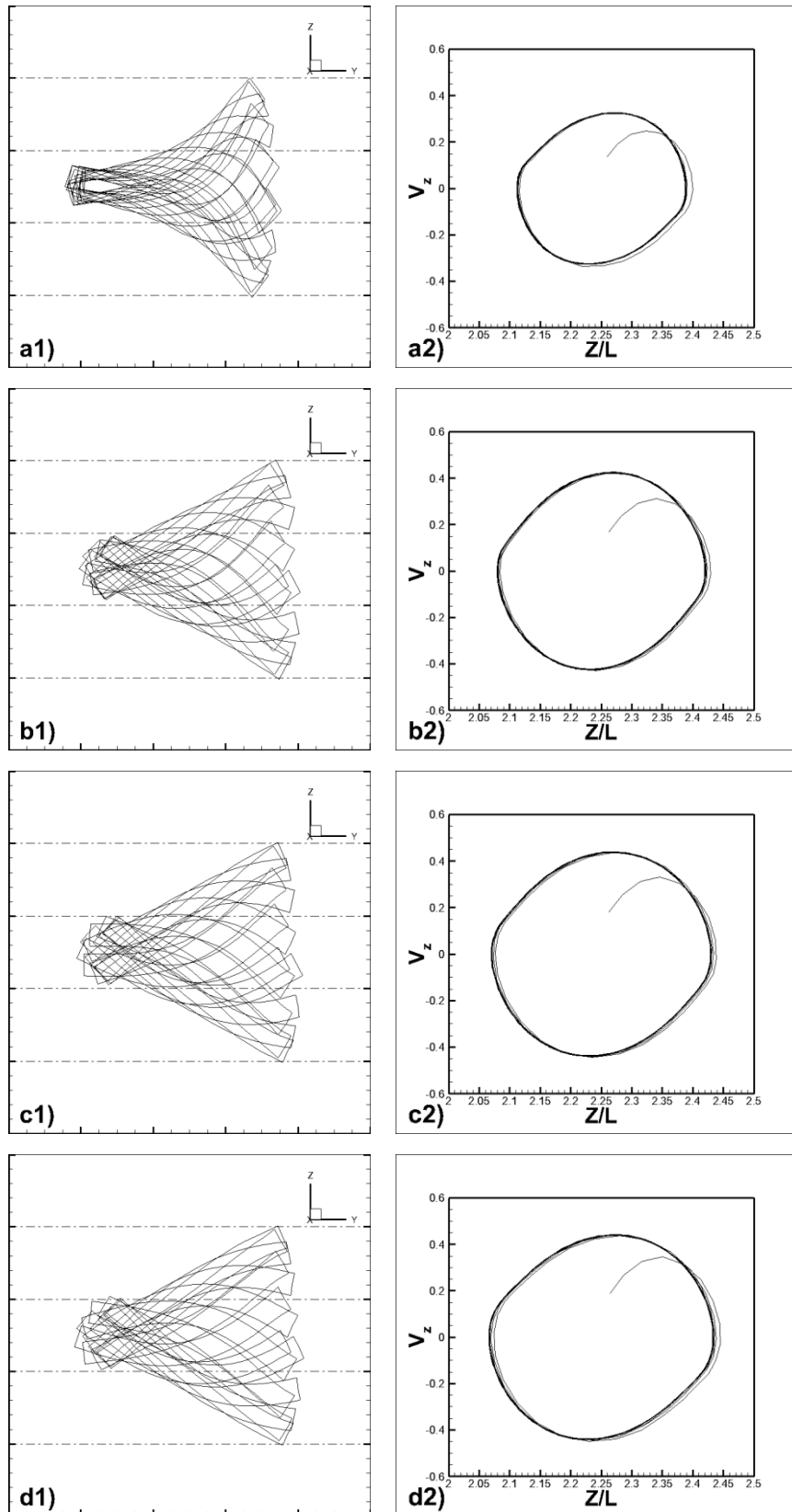


Figure 15 The flapping mode shape and the graph of V_z against Z/L (cases $Re=5$). Graphs a, b, c, and d correspond to cases of $EI = 0.035, 0.141, 0.211$ and 0.281 respectively. The flapping mode shape reflects the swimming body's locomotion in one period. The V_z - Z/L graph covers 16 period from first print step.

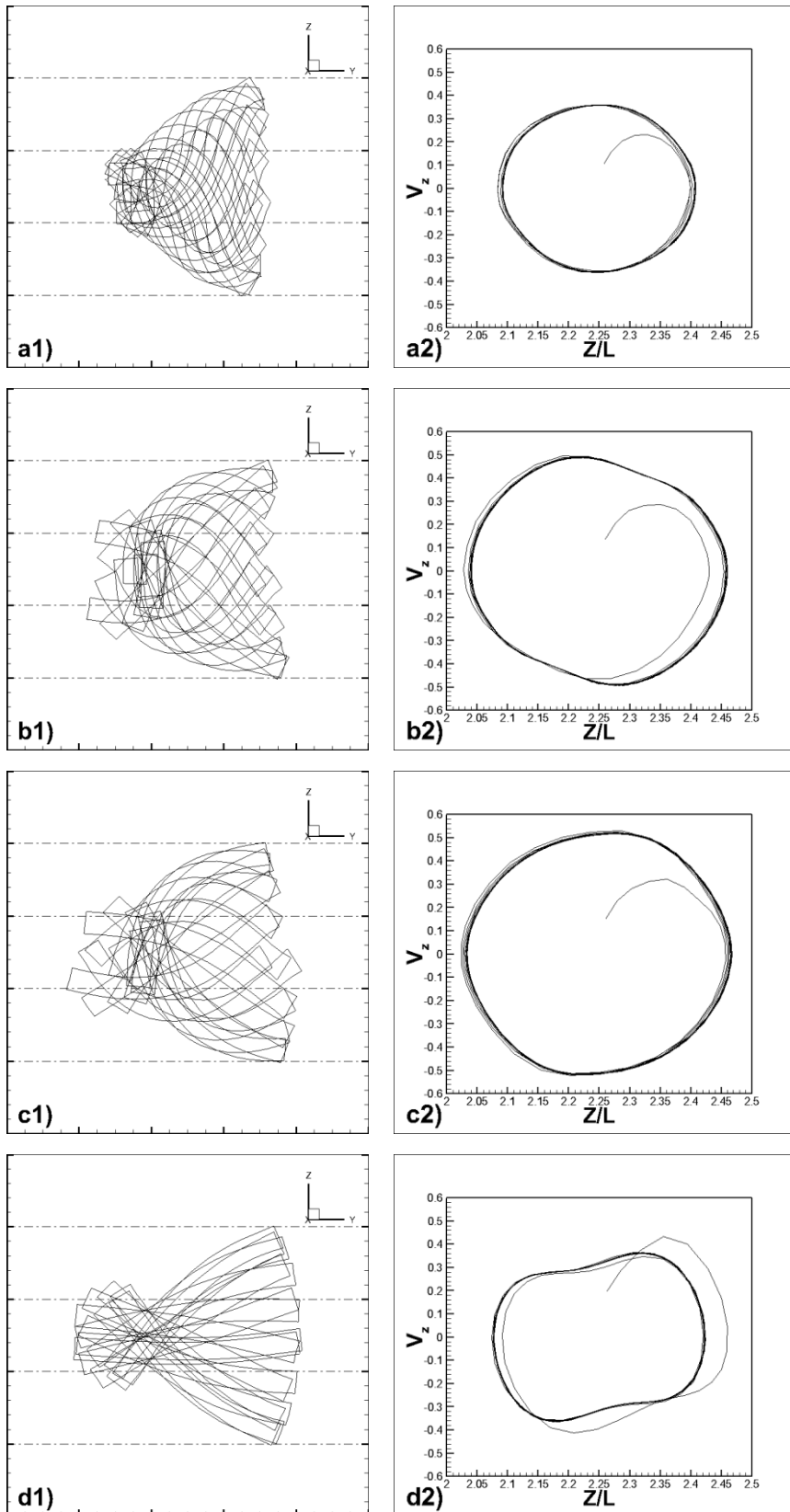


Figure 16 The flapping patterns for one period (case $Re=75$). Graphs correspond to cases of $EI = 0.008, 0.04, 0.08$ and 0.32 sequentially.

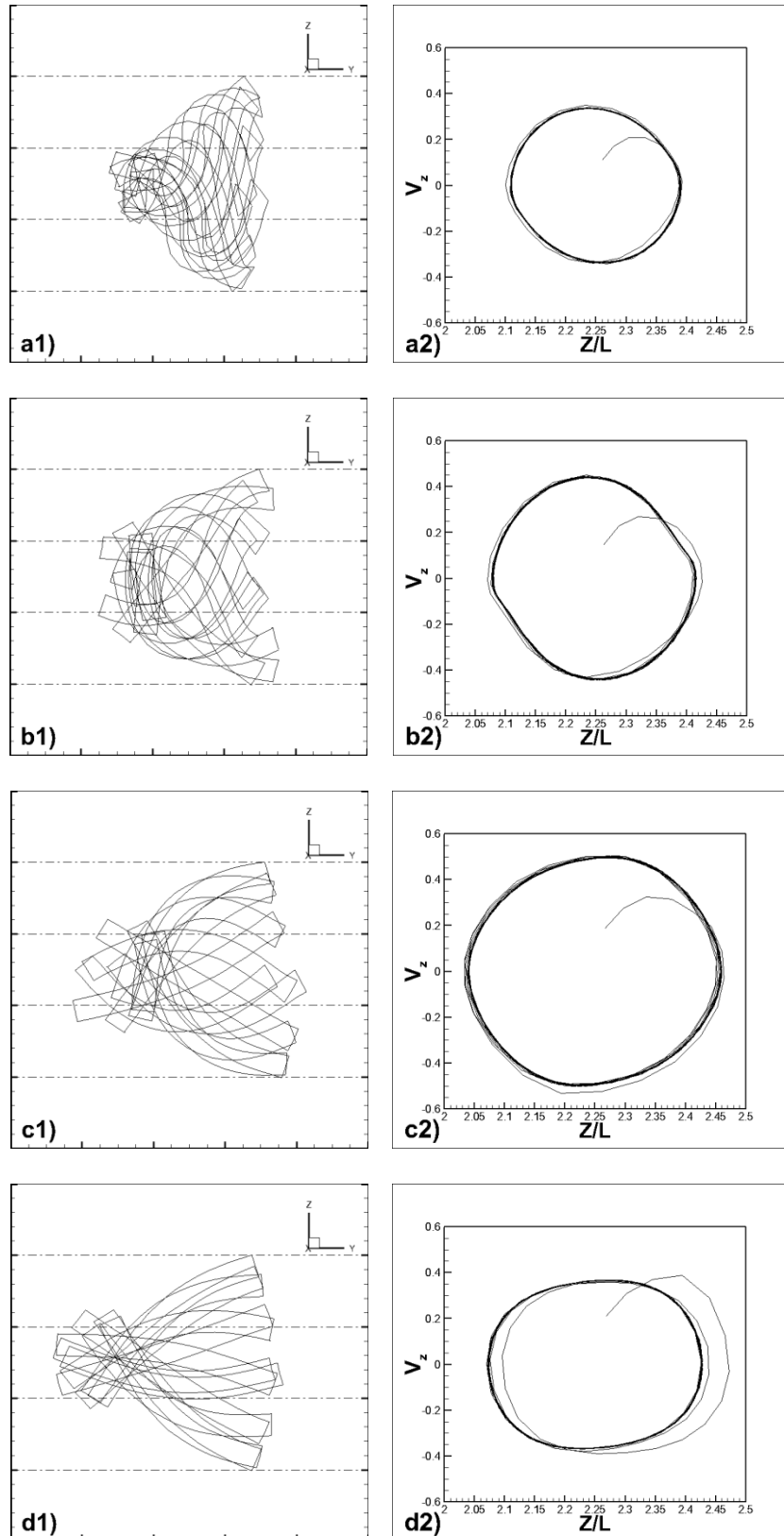


Figure 17 The flapping patterns for one period (case $Re=100$). Graphs correspond to cases of $EI = 0.004, 0.022, 0.087$ and 0.173 sequentially.

4.2 Two swimming bodies in tandem configuration

4.2.1 Equilibrium of separation distance

Figure 18 shows the evolution of separation distance between two swimmers. It is obvious that for both 0° phase difference and 90° phase difference simulation, an equilibrium separation distance can be achieved. In other words, for cases with same phase degree, the interactions through fluid flow field always push two tandem swimmers into a fixed separation distances. The basic physical explanation to this phenomenon is that the flow field caused by the front swimmer interferes with the rear one. And when two swimmers are close to each other, this kind of effect also reflects that the rear swimmer can act on front one.

For case A in figure 18 a), all cases with $\Delta\phi=0$ would achieve a same separation approximating 1.1, which we call the equilibrium state. Case with $D_{yi}=1.5$ only costs 24 periods to reach the equilibrium comparing to case with $D_{yi}=3$ costing more than 300 periods. This is because with increasing difference between D_{yi} and D_{eq} , the increasing time periods are needed to accumulate the interaction between two fibers to achieve balance. Same phenomenon can be found in Case B where $D_{eq}\approx 1.4$.

The reason why equilibrium gap distance can be achieved is that the rear swimming body is influenced by the wake of front swimming body and follows the “vortex locking” behavior[12]. The equilibrium gap distance is correlated with the streamwise period of the Karman vortex street. [26] [27]

Besides, two explanations should be pointed out. First, the line in figure 18 b) seems bold because of the vibrated gap distance. This is because we used center mass to locate the whole swimming body, when the phase difference is present, the location vibration caused by the different flapping period cannot be cancelled out each other. While the phase difference is absent, the location vibration is very tiny and can be ignored (see figure 18 a)). Second, no other equilibrium distances are found in this research. The interaction of any cases with a higher initial gap distance ($D_{yi}>4$) is too weak to observe.

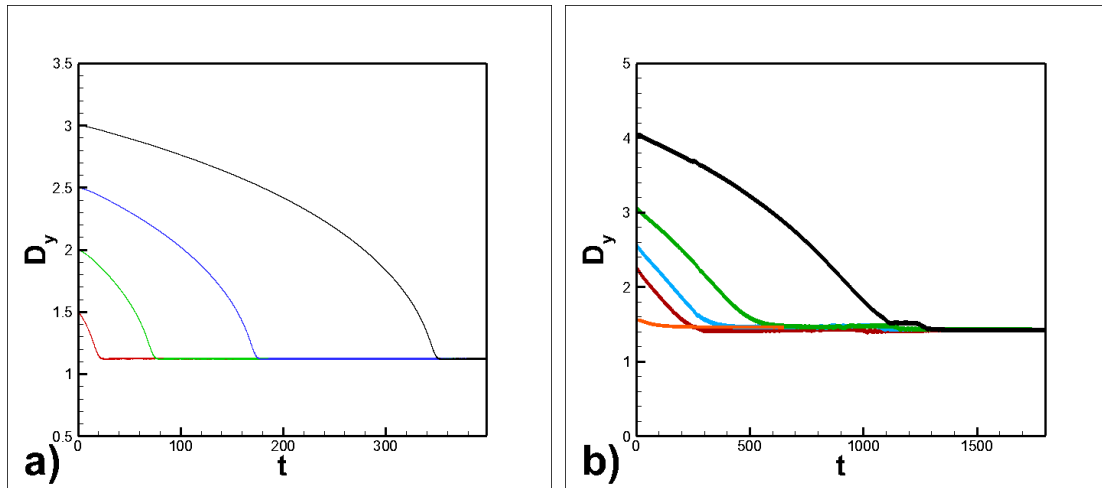


Figure 18 Separation distance as a function of time for a)case A and b)case B in Table 2.

4.2.2 Flow field analyses

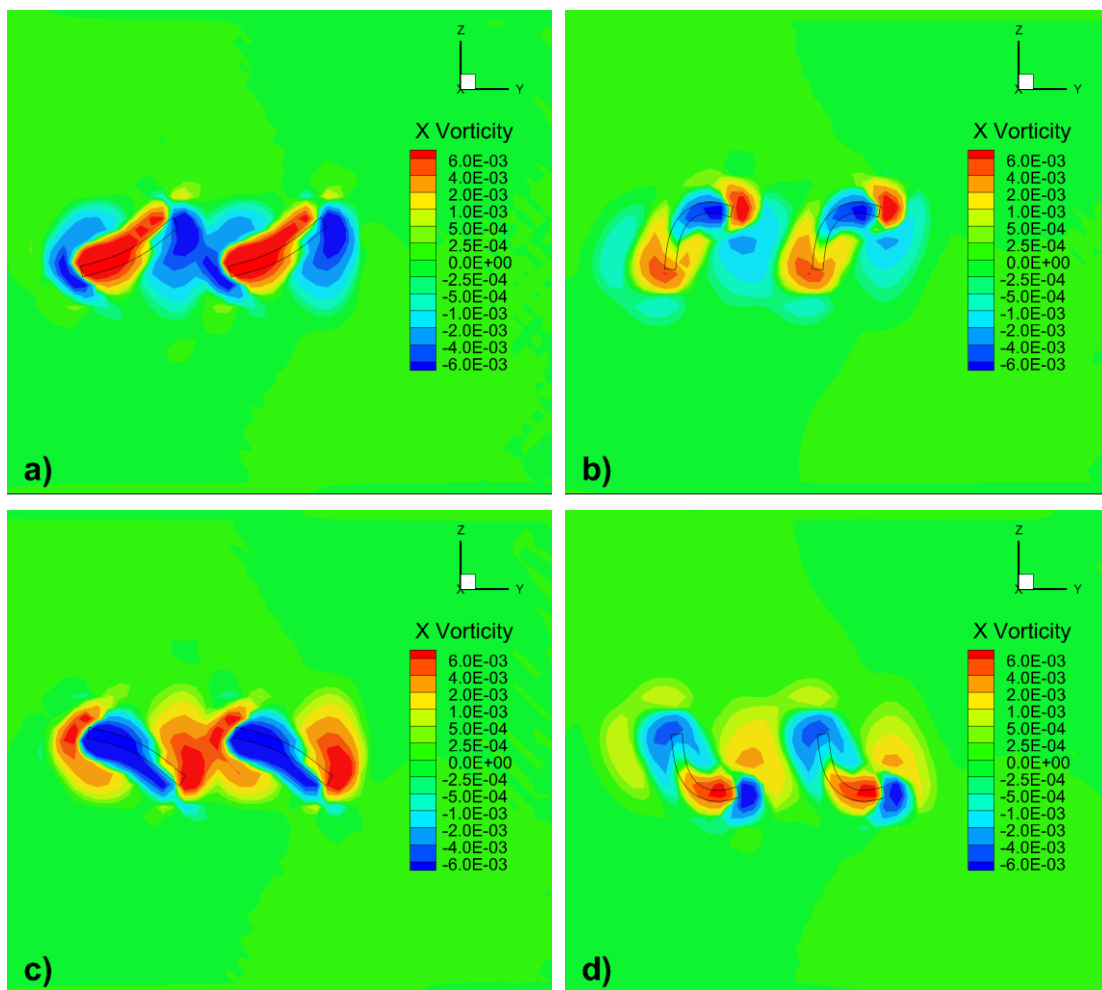


Figure 19 The fluid flow figure for cases with $Re=75$, $EI=0.08$, $\Delta\varphi=0$, $D_{yi}=1.5$.

Figure 19 shows the fluid flow patterns of in-phase case (which means $\Delta\phi=0$) in one flapping period. The locomotion of two swimmers in this case is fully synchronal. Then two identical flow patterns caused by two swimmers separately are formed. Meanwhile, being mentioned in previous section, the front swimmer influences the rear one. The evidences shown from the vorticity are, 1) overlapping occurs between the vortex at right end of rear swimmer and left end of front swimmer in figure 19 a) and c), 2) after the overlapping, the vertex at the right end of rear swimmer is larger than vertex at corresponding location of front swimmer (see figure 19 b) and d)), in which they should be exactly same if there is no flow-mediated interaction.

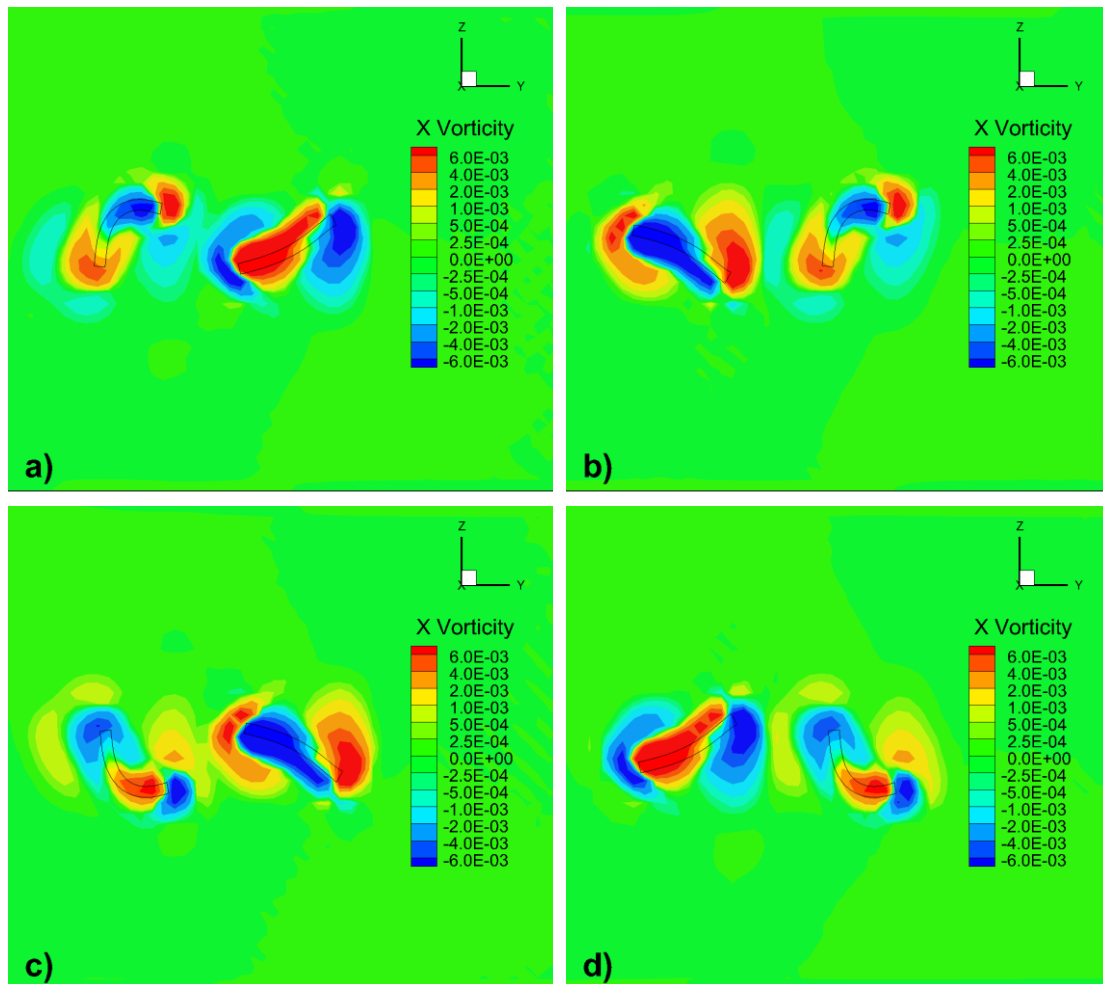


Figure 20 The fluid flow figure for cases with $Re=75$, $EI=0.08$, $\Delta\phi=90$, $D_{yi}=1.5$.

Figure 20 graphs the fluid flow patterns for case with $\Delta\phi=90$. Similar phenomenon is found. Two differences comparing to the in-phase case should be point out. First, the overlapping is not as obvious as occurred in the previous sample,

which means the rear swimmer receives a weaker flow-mediated interaction. It well explains why cases with phase difference cost more time to achieve equilibrium state than cases without phase difference do. Second, the comparing between two similar flow patterns in this case should be performed between two same mode shapes of solid swimming bodies. For instant, the front swimmer in figure 20 b) can be compared with the rear swimmer in figure 20 a).

5. Conclusions

Two new objects based on previous research are: a) Release the fixed head of bacteria to found new movement pattern; b) introduce more swimming bodies into whole simulation system. For the theoretical support in this research, Lattice Boltzmann Method, General Lattice Spring Model and Immersed-boundary Method are introduced to respectively simulate structure of fluid, solid and interaction between fluid and solid.

Before this study, seldom articles focus on undulation flapping in three dimension flow distribution at high Reynolds number. Lots of previous articles employed the traditional computational fluid dynamics methods (CFD) for fluid simulation.

Essentially, this research studies the locomotion patterns of solid swimming bodies in 3-D lattice Boltzmann flow field. In detailed, a self-propelled swimming body is driven by the vertical oscillation, and the simulation is performed in a 3-D fluid box. And Two-body system simulation begins with the initial setup of a tandem configuration. For each fiber, the setup is exactly same as that of single fiber.

To quantify the propulsive performance, some physical parameters are introduced such as normalized location Y/L , forward velocity V_y , flapping velocity V_z , cruising speed U_c , drag coefficient C_d , Power coefficient C_p , propulsive efficiency η , rigidity EI and Reynold number Re of solid swimming body.

In the section of flexibility effecting on periodic V_y , V_z , C_d and C_p , periodic graphs directly indicate the flapping locomotion pattern of swimming body in one period after reaching steady state.

In the section of flexibility effecting on U_c , C_p and η , the evolution of U_c , C_p and η along with increasing rigidity indicates existing of maximum. For all graphs in this section, same trends have been reported in previous article[12].

In the section of turning point of rigidity where the solid body travels from backward to forward, the results state that the swimming body migrates backward at

low rigidity and high Reynolds number. The mechanism of backward movement is also reported in [12], [22] and [23]. With low rigidity, the mode shape of swimming body is much different with a “standard” flapping mode shape. In the mode shape with low rigidity, the “tail” of swimmer forms overbending and pushes fluid forward and then propels itself backward. while for cases with low Reynolds number, the high viscosity of fluid restricts the forming of overbending and then backward stage is absent.

In the section of resonance, the role of relation between forcing frequency f and natural frequency f_0 is studied to optimize performance. For cases of high Reynolds number ($Re=75$ or 100), the maxima of U_c and C_p are located in the domain around 1 ($f=0.7-1.3$). The results successfully suggest resonance plays a critical role on flapping, which accords with many researches in the field of aerodynamics or fluid dynamics such as [24].

In the section of mode shape, graphs of V_z against Z/L are introduced to quantify the flapping patterns of solid body. With graphs of mode shape, it is feasible to explore the mechanism such as backward movement and existing of maximum of cruising speed.

Two-body system is also studied in this research and results are reported and compared with previous study in 2-D flow field by traditional methods[13]. Under the tandem configuration, for both 0° phase difference and 90° phase difference simulation, an equilibrium separation distance can be achieved. In other words, for cases with same phase degree, the interactions through fluid flow field always push two tandem swimmers into a fixed separation distances. The reason why equilibrium gap distance can be achieved is that the rear swimming body is influenced by the wake of front swimming body and follows the “vortex locking” behavior[12]. The equilibrium gap distance is correlated with the streamwise period of the Karman vortex street. [26] [27]

The fluid flow patterns of 0° -phase-difference case and 90° -phase-difference case are presented. Fluid flow figures indicate the degree of influence between two swimmers. The results state case without phase difference has a stronger interaction

than case with 90° phase difference. It explains that the later cost more time period to achieve balance gap distance.

REFERENCES

- [1] Wu T, Guo R, He G, Liu Y, Qi D. 2013, Simulation of swimming of a flexible filament using the generalized lattice-spring lattice-Boltzmann method. *Journal of Theoretical Biology* 22, 349 (2014) 1-11.
- [2] Taylor G. 1951, Analysis of the swimming of microscopic organisms. *Proc R Soc Lond B Biol Sci* 209, 447–461.
- [3] Machin K E. 1958, Wave propagation along flagella. *J. Exp. Biol.* 35.
- [4] Purcell E M. 1977, Lift at low Reynolds number. *American Journal of Physics* 45.
- [5] Wiggins C H, Goldstein R E. 1998, Flexible and propulsive dynamics of elastica at low Reynolds number. *Phys. Rev. Lett.* 80.
- [6] Wiggins C H, Chris H, Rivelino D, Ott A, Goldstein, Raymond E. 1998, Trapping and wiggling: Elastohydrodynamics of driven microfilaments. *Biophysical Journal* 74.
- [7] Yu, Tony S., Lauga, Eric & Hosoi, A. E. 2006 Experimental investigations of elastic tail propulsion at low Reynolds number. *Phys. Fluids* 18.
- [8] Pak, On Shun, Gao, Wei, Wang, Joseph & Lauga, Eric 2011 High-speed propulsion of flexible nanowire motors: Theory and experiments. *Soft Matter* 7, 8169–8181.
- [9] Lagomarsino, M. C., Capuani, F. & Lowe, C. P. 2003 A simulation study of the dynamics of a driven filament in an Aristotelian fluid. *J. Theor. Biol.* 224.
- [10] Eric, Lauga & Powers, Thomas R. 2009 The hydrodynamics of swimming microorganisms. *Rep. Prog. Phys.* 72.
- [11] Ishikawa, T. Sekiya, G. Imai, Y. and Yamaguchi, T.. 2007. Hydrodynamic Interactions between Two Swimming Bacteria. *Biophysical Journal* Vol.93 2217–2225
- [12] Xiaojue Zhu, Guowei He, Xing Zhang. 2014. Numerical study on hydrodynamic effect of flexibility in a self-propelled plunging foil. *Computers & Fluids* 97 (2014) 1–20
- [13] Xiaojue Zhu, Guowei He, Xing Zhang. 2014. Flow-Mediated Interactions between Two Self-Propelled Flapping Filaments in Tandem Configuration. *PHYSICAL REVIEW LETTERS*, DOI: 10.1103/PhysRevLett.113.238105
- [14] Feng, Zhi-Gang & Michaelides, Efsthios E. 2004 The immersed boundary-lattice Boltzmann method for solving fluid-particle interaction problems. *Journal of Computational Physics* 195, 602–628.
- [15] Wu, Jingshu & Aidun, Cyrus K. 2010 Simulating 3d deformable particle suspensions using lattice Boltzmann method with discrete external boundary force. *Int. J. Numer. Meth. Fluids* 62, 765–783.
- [16] Peskin, Charles S. 2002 The immersed boundary method. *Acta Numerica* pp. 479–517.
- [17] Buxton, Gravin A., Verberg, Rolf, Jasnow, David & Balazs, Anna C. 2005 Newtonian fluid meets an elastic solid: Coupling lattice Boltzmann and lattice-spring models. *PHYSICAL REVIEW E* 71.
- [18] Qi, Dewei, Liu, Yingming, Shyy, Wei & Aono, Hikaru 2010 Simulations of dynamics of plunging and pitch of a three-dimensional flexible wing in a low Reynolds number flow. *PHYSICAL OF FLUIDS* 22.
- [19] Liu, Yingming, Wu, Tai-Hsien, Guo, Rung-Sheng, Lee, Yi-Hsuan & Qi, Dewei 2011 Dynamics of sedimentation of flexible fibers in moderate Reynolds number flows. *Computers & Fluids* 48.
- [20] Lee J, Lee S. Fluid-structure interaction for the propulsive velocity of a flapping flexible plate

at low Reynolds number. *Comput Fluids* 2013;71:348-74.

- [21] GRAY J. and G. J. HANCOCK, 1995. The Propulsion of Sea-Urchin Spermatozoa. *J Exp Biol* 32, 802-814.
- [22] Spagnolie SE, Moret L, Shelley MJ, Zhang J. Surprising behaviors in flapping locomotion with passive pitching. *Phys Fluids* 2010;22:041903.
- [23] Zhang J, Liu NS, Lu XY. Locomotion of a passively flapping flat plate. *J Fluid Mech* 2010;659:43-68.
- [24] Hassan Masoud, Alexander Alexeev. 2012. Efficient Flapping Flight Using Flexible Wings Oscillating at Resonance. *The IMA Volumes in Mathematics and its Applications*. Volume 155, 2012, pp 235-245
- [25] J. C. Liao, D. N. Beal, G. V. Lauder, and M. S. Triantafyllou, Fish Exploiting Vortices Decrease Muscle Activity, *Science* 302, 1566 (2003).
- [26] L. B. Jia and X. Z. Yin, 2008, Passive oscillations of two tandem flexible filaments in a flowing soap film. *Phys. Rev. Lett.* 100, 228104 (2008).